The Influence of Wedge Angle, Feedstock Color, and Infill Density on the Color Difference of FDM Objects

Ali Payami Golhin and Are Strandlie

Department of Manufacturing and Civil Engineering, Norwegian University of Science and Technology, 2815 Gjøvik, Norway
E-mail: payami.ag@gmail.com

Philip John Green▲

Department of Computer Science, Norwegian University of Science and Technology, 2815 Gjøvik, Norway

Abstract. *The surface appearance in additive manufacturing (AM) has attracted attention in recent years due to its importance in evaluating the quality of 3D printed structures. Fused Deposition Modeling (FDM), also known as Fused Filament Fabrication (FFF), holds an important share of the AM market because of its large economic potential in many industries. Nevertheless, the quality assurance procedure for FDM manufactured parts is usually complicated and expensive. The enhancement of the appearance at different illumination and viewing angles can be exploited in various applications, such as civil engineering, aeronautics, medical fields, and art. There are two steps in improving the microstructure and material appearance of printed objects, including pre-processing and post-processing. This study aims to elucidate the role of the pre-processing phase in the development of FDM parts through the assessment of color differences. For this purpose, a set of polymeric samples with different wedge (slope) angles were 3D printed using an FDM printer. The color difference between the elements is discussed and correlated with the pre-processing parameters. It is revealed that the wedge angle of the elements in the design, slicing process, and infill density could alter the color appearance of the printed parts in a predictable trend. This research suggests that low infill density and wedge angles in polylactide filaments can result in a more stable color appearance.* © *2021 Society for Imaging Science and Technology.*
[DOI: 10.2352/J.ImagingSci.Technol.2021.65.5.050408]

1. INTRODUCTION

The introduction of additive manufacturing (AM) has given rise to many new possibilities. It is a complementary option to the subtractive methods that have dominated the manufacturing and production sector since the first industrial revolution. AM offers improved functional device integration capabilities, thanks to a wide range of 3D geometry, ranging from micrometers to centimeters [1]. The fast-paced AM marketplace has also shifted from industrial applications to customized manufacturing. The variation in color property can deeply influence the customized product to some extent, which is also known as the subdivision of color 3D printing [1]. Full-color 3D printing and accurate color reproduction are highly desired when 3D objects were manufactured by AM techniques. On this basis, color fidelity and color preference have significant influence on the overall quality of the product [2].

Color 3D printing is gaining increasing popularity in recent years, as it enables customized production in various industrial applications based on different substrates, including plastic [3–7], powder [8, 9], paper [10–14], metal [15, 16], glass [17], food [18], and organism [19]. While the seven categories of applications for color 3D printing techniques range from processes to coloring materials in 3D printing, they follow the same subtractive color theory standardized by the CIE (Commission Internationale de L'Eclairage) and the ICC (International Color Consortium) for 2D printing. The quality of surface colors of AM objects can be evaluated based on color stability and color reproduction methods. Nevertheless, the procedures for evaluating 3D objects are less than traditional 2D objects, demanding a detailed guideline for managing the color process of 3D printed objects [1].

The instrumental measurement geometry is one of the critical factors when it comes to color measurement. Since there is no CIE standard for the measurement of 3D prints, appearance measurement for AM technology requires careful considerations due to the variation in color and illumination geometries [20]. However, several attempts have been made to develop appearance assessments for 3D color printing processing [7, 19, 21–23]. Accordingly, a framework of color image reproduction for 3D color printing has been introduced by Xiao et al. [2]. They proposed that the performance of color reproduction can be significantly improved by applying the framework.

There are several AM technologies that can be classified as color 3D printing with the full-color spectrum, including Color FDM and PolyJet introduced by Stratasys Inc., MultiJet Fusion from Hewett Packard Inc.p, SDL processing from Mcor Inc. and 3DP developed by Z Corp Inc. and 3D system Inc. MultiJet Fusion 3DP, and SDL processing are based on the 3D printing of CMY(K) ink on printing materials with a single color, while Color FDM and PolyJet require colored feedstocks in order to generate a full color by melting materials together. This is a complex project which makes color 3D printing generally more sophisticated than conventional color printing technologies [2].

According to ISO/ASTM standard 52,900:2015, fused deposition modeling (FDM) is classified as a material
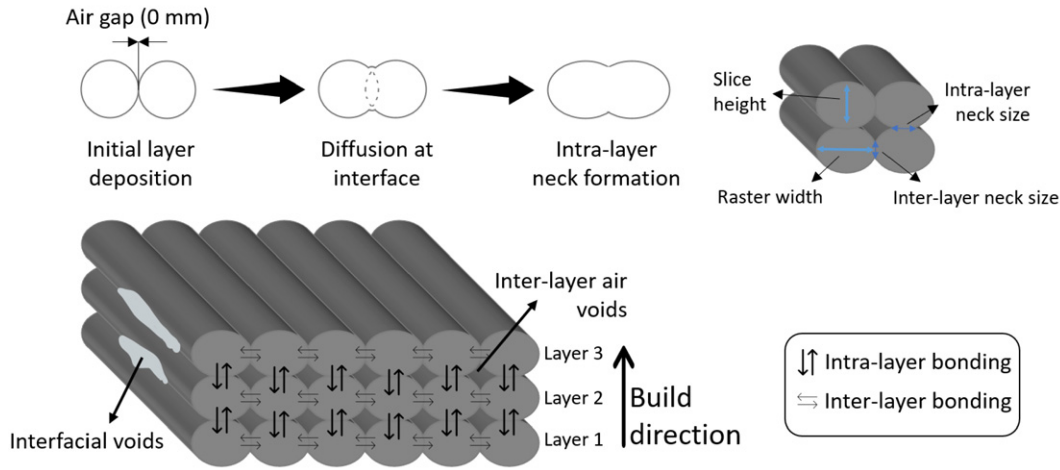
Figure 1. Bonding and stages of bond formation in the FDM process.

extrusion-based AM technique [24]. FDM is the most economical technique among other AM methods due to its advantages such as the high strength of its materials, cost-effectiveness, ease of printing, multicolor and glossiness appearance, and environmentally friendly nature [25, 26]. In this regard, FDM is an excellent candidate for biomedical, marine, and aerospace applications such as mechanical housings, antennas, satellites, thermal management components, and unmanned aerial vehicles (UAV) [4–6].

While the developments of FDM 3D printing and the mechanical properties of printed polymers have been remarkable thus far [27–29], manufactured objects tend to suffer from the inferior surface quality, including undesirable color variation, pronounced striations, high roughness, and voids [30]. In other words, the smoothness, precision, and topography of FDM parts are not comparable with some other AM techniques such as PolyJet and Multi-Jet [29]. FDM objects are printed in a layer-upon-layer routine after the successive completion of each cross-section based on the computer-aided design (CAD) data [25, 31]. Thus far, this is not the sole reason that explains the drawbacks of this technique. This is primarily caused by the filamentary nature of the FDM technique. For instance, high-temperature variation during layer by layer part fabrication procedure and inappropriate infill density can affect the print quality [30]. Morphology is poor due to various limiting factors such as phase transformations, rapid cooling, and exhaustive energy. Moreover, the FDM printed parts deviate from the initial geometry, as well as volumetric errors and hardware settings [32–35].

On top of all these limitations, FDM is a dominant AM technique in the market due to its various advantages, including cost, printing time, bio-degradable materials, and simplicity [25].

The FDM parts require significant post-production finishing techniques (PPFTs) to meet its large market [25]. For a variety of applications, manufacturers use coating and painting methods to obtain the desired surface finish.

However, these techniques pose several challenges that need to be overcome to form the printing process. For example, there is an accumulation problem along the edge of the object and then inside the part at the beginning of the FDM process. This problem cannot be solved by coating or painting since it requires a specific number of outlines to package the part according to the required response [25, 36].

In general, two types of bonding exist in the FDM process, including inter-layer and intra-layer bonding. The high thermal expansion of pure polymers creates a loose bond between the layers during printing, leading to the formation of the staircase (Figure 1). As an inherent issue, the formation of staircases has a significant negative influence on the surface appearance of FDM parts [9–13].

The infill density defines the level of incorporating material inside the fabricated object. It may vary from 0 to 100%, depending on the required balance between material consumption and mechanical properties [10]. Generally, a higher infill density leads to a heavier and stronger part, which increases the cost and the material used for the printing process. The density and pattern of infill are important process parameters that can influence the surface quality as well. As such, they should be selected appropriately considering the design and strength requirements, as well as the build time of the printed part [2]. For instance, surface artifacts such as gaps and porosity have been observed even at 100% infill density under a scanning electron microscope (SEM) [11].

There is a wide range of filaments in the market with different colors, however, 3D printing contains unreal tristimulus values based on standard color charts compared to the designed CAD file. In order to calculate the color difference between two objects, the CIE recommended two alternates for RGB, including CIELCH (L^*C^*h) and uniform color scales: CIE 1976 ($L^*a^*b^*$) or CIELAB. The CIE76 (ΔE_{ab}) formula was the first color-difference formula based on CIELAB values. It has been succeeded by the CMC (Color Measurement Committee) in 1984 and followed by improvement in CIE94 and CIEDE2000 formulas [37, 38],
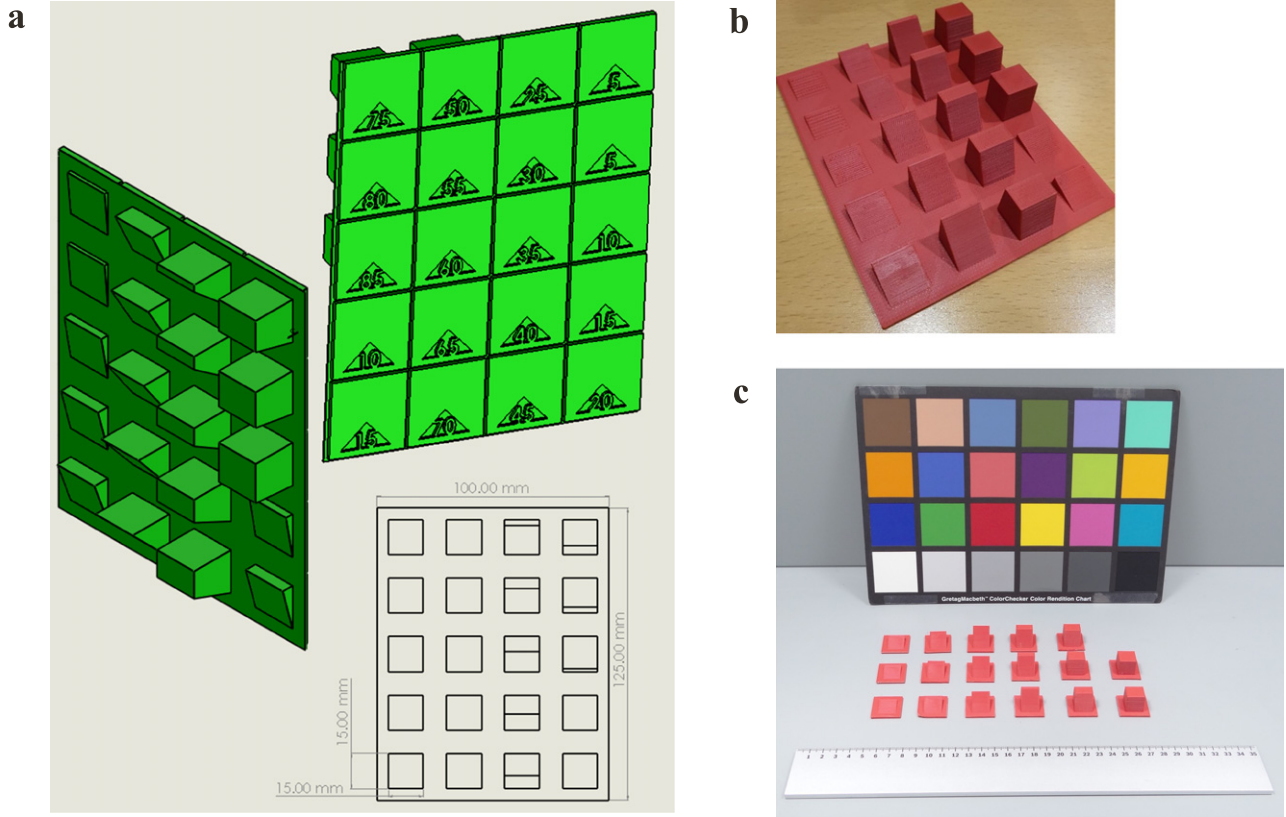
Figure 2. (a) The design, (b) as-3D printed model, and (c) separated specimens with different wedge angles placed in a light box under D50 light source. The sample was printed using a red PLA filament with an infill density of 0%.

whereby

$$\Delta E_{ab}^* = \sqrt{(\Delta L^*)^2 + (\Delta a^*)^2 + (\Delta b^*)^2} \quad (1)$$

$$\Delta E_{CMC}^* = \sqrt{\left(\frac{\Delta L^*}{lS_L}\right)^2 + \left(\frac{\Delta C^*}{CS_C}\right)^2 + \left(\frac{\Delta h^*}{S_h}\right)^2} \quad (2)$$

$$\Delta E_{94}^* = \sqrt{\left(\frac{\Delta L^*}{k_L S_L}\right)^2 + \left(\frac{\Delta C^*}{k_C S_C}\right)^2 + \left(\frac{\Delta h^*}{k_h S_h}\right)^2} \quad (3)$$

$$\Delta E_{2000}^* = \sqrt{\left(\frac{\Delta L^*}{k_L S_L}\right)^2 + \left(\frac{\Delta C^*}{k_C S_C}\right)^2 + \left(\frac{\Delta h^*}{k_h S_h}\right)^2 + R_T f(\Delta C^* \Delta h^*)}, \quad (4)$$

where LCh is Lightness (the same one as in $L^*a^*b^*$), chroma (the distance out from the neutral axis – saturation) and hue, the constant values of k_L (lightness), k_C (chroma), and k_h (hue) in computer graphic arts are usually unity [39]. Other parameters refer to the hue rotation term (R_T), and the compensation for lightness (S_L), chroma (S_C), and hue (S_h). CIEDE2000, as the most recent formula, has become the recommended industry standard for all calculations except textiles, which still use CMC [40].

Knowledge of color science is crucial for the success of 3D printed parts. While color stability and the appearance of 3D surfaces have been reported [15], studies of color differences based on the printing processes are lacking. Therefore, this study aimed to evaluate the influence of the CAD design and the slicing parameters in the pre-processing stage on the color difference of FDM objects. Accordingly, we emphasize a method to deliberately alter the color appearance of 3D printed surfaces by controlling the generation of texture in the pre-processing stage for polylactice (PLA) filaments.

2. DESIGNS AND METHODS
Due to feasibility and a broad application of SolidWorks in additive manufacturing, the structured surface models were created in SolidWorks CAD 2020 (Dassault Systems, Velizy, France) in the native format (*.sldprt) and subsequently imported to the Prusa Slicer for the slicing process. Both software are well known CAD systems of the manufacturing community due to their ease of use and extended functionality unavailable in open source software [15].

The design and appearance of the 3D-printed model, together with separated wedge specimens, are displayed in Figure 2. All separated wedges were stored in the as-printed state without post-processing after 3D printing. To focus on the role of design features and the color attribute, "blue" and "red" matte filaments have been used to print physical models. In order to decrease the influence of the printing layout of samples with different wedge angles (distribution at a work platform) on the surface properties, a high density of parts with reduced size in the base area (15×15 mm) is chosen as the main design criterion.
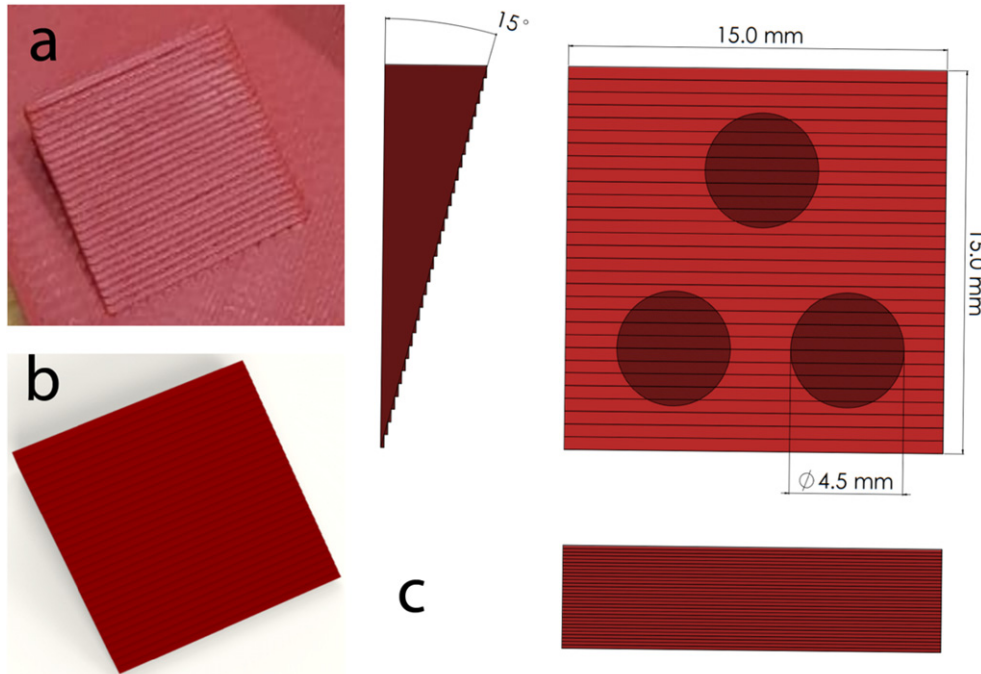
Figure 3. (a) The 15° wedge angle feature on the dull red sample 15, (b) the twin digital model, and (c) measurement positionings of the 4.5 mm aperture on the surface.

This means that these features are positioned as closely together as possible, while they could be split easily. Additional attention was paid to wedge angles 5°, 10°, and 15°. These tilted surfaces were duplicated in the design at different locations on the build platform, and recognizing staircase problems were more critical for low-wedge angles.

The CAD model was exported using the fine STL from SolidWorks (tolerance 0.12 mm) to be read and interpreted by the print setup software. G-codes were obtained using PrusaSlicer 2.2.0 software in the slicing step. 3D printing was performed using a Prusa i3 MK2.5 3D printer with a 0.4 mm nozzle, layer heights from 0.15 mm at the bottom and 0.07 mm at the studied wedge features, step size in X/Y axis -0.01 mm, maximum speed 200 mm/s, and the working area of $250 \times 210 \times 210$ mm^3. PLA filaments were sourced from add:north, Sweden. The X-PLA filament had a diameter of 1.75 mm (diameter tolerance 0.025 mm) in two matte colors of red and blue. Although these colors were stated by the manufacturer, the printed blue color was more of a cyan color, and red was reproduced in dull red. Thus, they would be so-called cyan and dull red from in this paper. Wedge angles from 0 to 90 at 5 degrees intervals were printed using these two colors feedstocks and for each different infill density. The adjustable maximum and minimum infill densities were limited to 0 and 90%, and it was not possible to apply more than 90% for this design. The values of 30 and 60% were also applied to track the role of this pre-processing parameter on the surface color.

The spectral diagrams on the surface of the printed FDM part were measured by a spectrophotometer (X-Rite i1 Pro, Switzerland) under a D50 light source. A 45:0 degree viewing geometry under the standard CIE Publication 15.2 was used to study the surface of the 3D-printed wedges. The optical resolution and physical sampling interval within the 380–730 nm spectral range were 10 and 3.5 nm, respectively. Calibration was performed with the standard white ceramic patch of the device before each series of measurements. To avoid errors due to other sources of light, all measurements were done in a dark room. The rear side of the instrument was kept rested on a planar surface, and the aperture was placed perpendicular on three different areas of sample surfaces (hatched circles in Figure 3c) to ensure the correct optical angles. The trend in the spectral results has been controlled using a tele-spectroradiometer (TSR) model CS-2000 from Konica Minolta assessing samples at the same 45:0 geometry, placed in a D50 light box. The TSR lens was perpendicularly positioned by a 1° field of view at a distance of 50 cm from the target specimens.

The results were averagely extracted from at least three times of measurements for each wedge. The minimum thickness per raster/layer on the surface (print resolution) was 0.07 mm. It is estimated that a minimum of eight layers was investigated for each measurement. Finally, the color difference (ΔE_{ab}^*) values were calculated using a color engineering toolbox in MatLab [15].

All data files were recorded in $L^*a^*b^*$, LCh, and XYZ using ColorPort 2.0 software in order to overcome the limitations of chromaticity diagrams like RGB in this study. Therefore, all spectral diagrams were extracted from the measurement directly. Finally, the color difference values were calculated using the Eq. (4) of CIEDE2000, where the parametric factors for K_L, K_C, and K_H were set to 1 [41].

3. RESULTS AND DISCUSSION

The i1Pro spectrophotometer used in this study was inspected and tested to examine the intrinsic error caused by the measuring device. Figure 4 provides the spectral results and color different specifications based on 25 measurements of the standard ceramic tile (white reference) under D50 illumination.
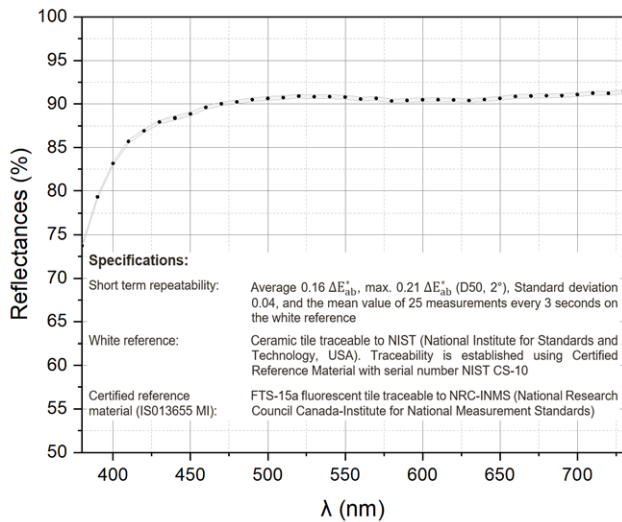

Figure 4. The average spectral and corresponding standard deviation area of the spectrophotometer. The attached specifications represent the reproducibility of the measurements and measurement uncertainty.

Spectral results of the cyan FDM samples at different infill densities are shown in Figure 5. The distributed reflectance spectra were recorded from the wavelength of 380 to 730 nm at intervals of 10 nm. As can be seen, the reflectance behavior is almost the same at different wedge
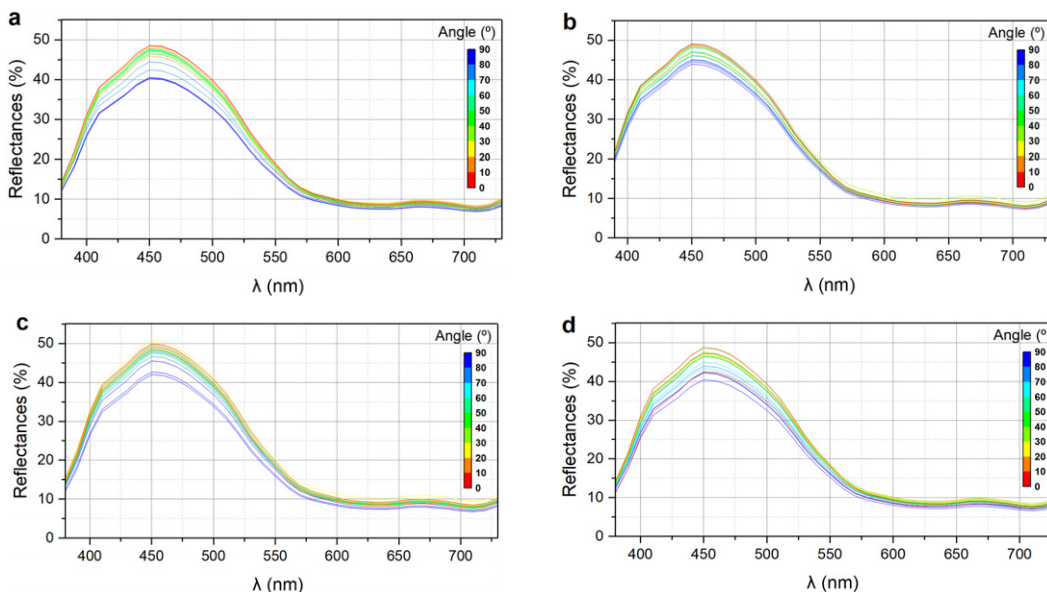
angles and infill density and limited to values between approximately 5 and 55%. However, the graphs shifted to a lower level by increasing the wedge angle. It means that the 0° and 90° had the maximum and minimum reflectance values, respectively and eventually confirmed by the higher lightness value (L) in $L^*a^*b^*$ values.

In this work, the procedures attempted to follow ISO/TS 23031:2020 (E) [16]. Thus, the evaluation of the spectral differences between the reference and test spectra, and the corresponding color difference, could be performed with the root-mean-square error (RMSE) and mean color differences from the mean (MCDM), respectively [17, 18]. The definitions are as follows.

$$\text{RMSE} = \sqrt{\frac{1}{N} \sum_{i=1}^{N} (r_{r,i} - r_{t,i})^2} \qquad (5)$$

$$\text{MCDM} = \frac{1}{N} \sum_{i=1}^{n} \Delta E(C_i, C_m)^2, \qquad (6)$$

where N is the number of reflectance readings, r_r and r_t are the references and test spectrum. C_i and C_m are the CIELAB color coordinates of the ith readings and the average reflectance of all readings, respectively.

Figure 6 represents the chromaticity coordinates of each sample on different wedges. As illustrated in Figure 7, when the infill density was fixed, the distribution of $x–y$ values for angle 0° was almost in the same range in the case of different infill densities. However, the distribution for the rest angles barely followed a certain pattern.

The color characteristics results in Figures 8–10 give the same interpretation as the chromaticity diagram results. In Fig. 9, infill densities of 0% and 90% represent a larger color gamut compared to other cyan samples. The size and
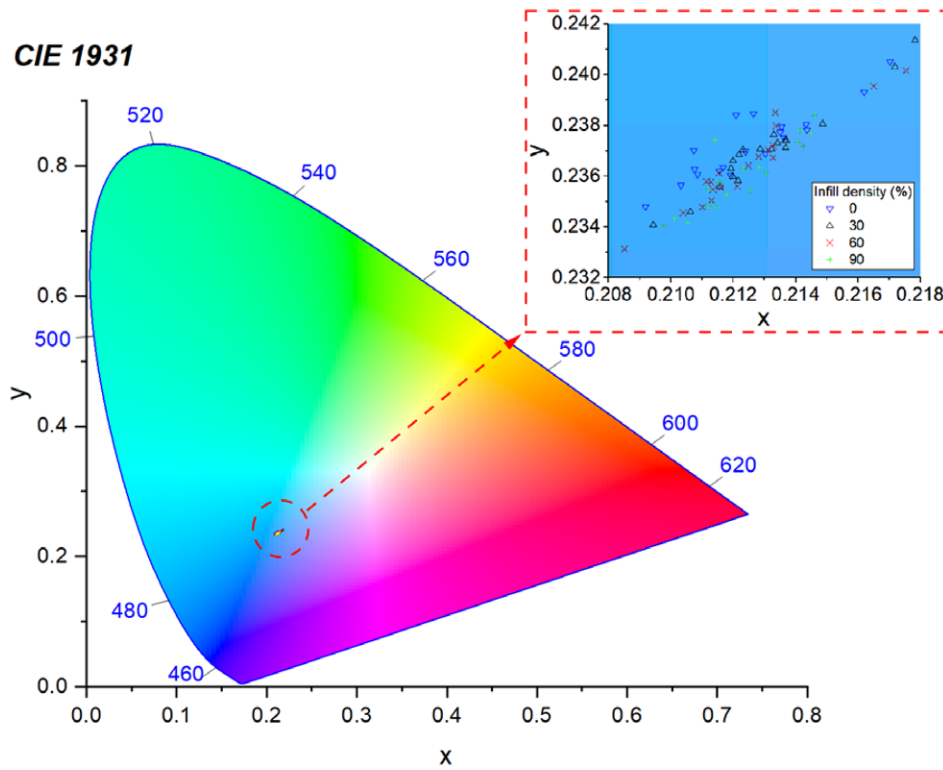

Figure 5. Reflectance spectra of cyan FDM specimens at different infill densities: (a) 0, (b) 30, (c) 60, and (d) 90%.

Figure 6. The enlarged and the chromaticity coordinates of the cyan samples at different wedges according to the CIE 1931 $x-y$ chromaticity diagram (D50).
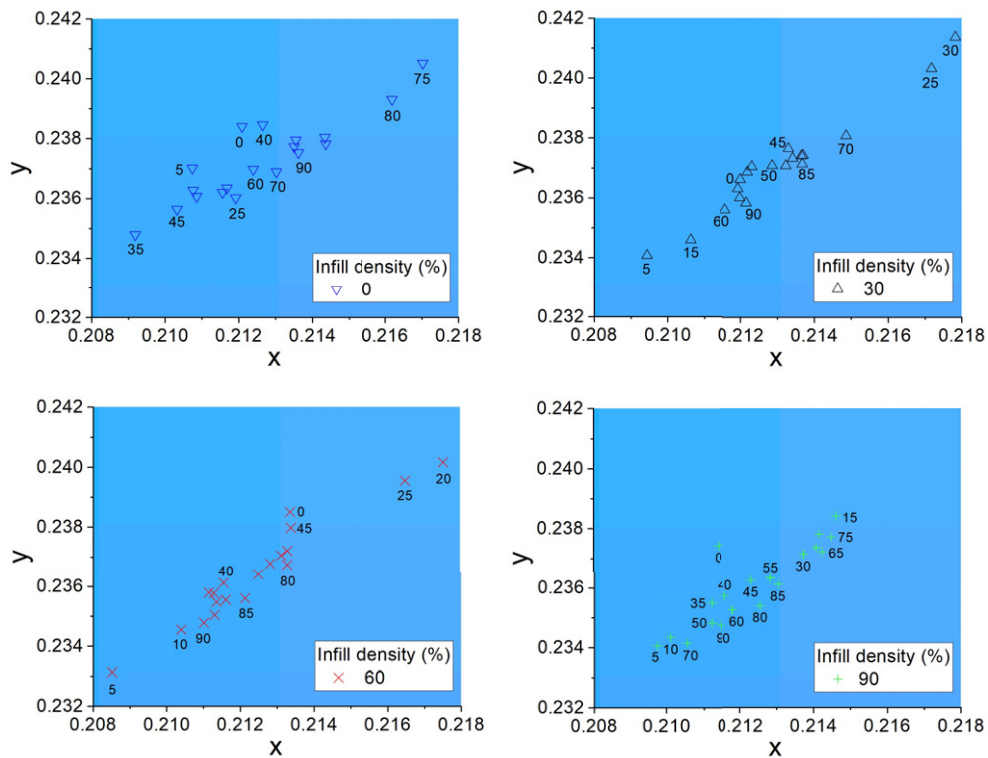
Figure 7. The chromaticity coordinates of the cyan samples at different infill densities according to the CIE 1931 $x-y$ chromaticity diagram (D50).

direction of color change in selected wedge angles in Fig. 10 reveal the CIEDE2000 color difference and the a^* and b^* direction according to the reference sample at 0° angle.

Generally, it can be seen that the color change in a^*b^*-plane for higher wedge angles was more significant than the lower angles at different infill densities (Fig. 10).

a

	Wedge angle					
	0°	20°	40°	60°	80°	90°
L*	51.3	51.2	50.3	50.6	47.6	47.0
a*	-15.4	-14.2	-14.9	-14.5	-13.0	-13.4
b*	-37.8	-37.7	-37.2	-37.8	-35.1	-35.5
C	40.8	40.2	40.1	40.5	37.4	38.0
h°	247.9	249.4	248.1	249.0	249.7	249.3

b

	Wedge angle					
	0°	20°	40°	60°	80°	90°
L*	51.3	50.2	51.1	50.1	49.3	48.7
a*	-14.8	-14.5	-14.7	-14.3	-13.9	-13.8
b*	-38.4	-37.8	-38.1	-38.1	-36.9	-37.1
C	41.1	40.5	40.8	40.7	39.4	39.6
h°	248.9	249.1	248.9	249.4	249.3	249.6

c

	Wedge angle					
	0°	20°	40°	60°	80°	90°
L*	52.0	52.8	51.1	50.2	49.6	47.5
a*	-15.0	-13.8	-14.8	-14.3	-13.8	-13.7
b*	-38.0	-37.5	-38.4	-38.3	-37.3	-36.8
C	40.8	40.0	41.2	40.9	39.8	39.3
h°	248.5	249.9	249.0	249.6	249.6	249.6

d

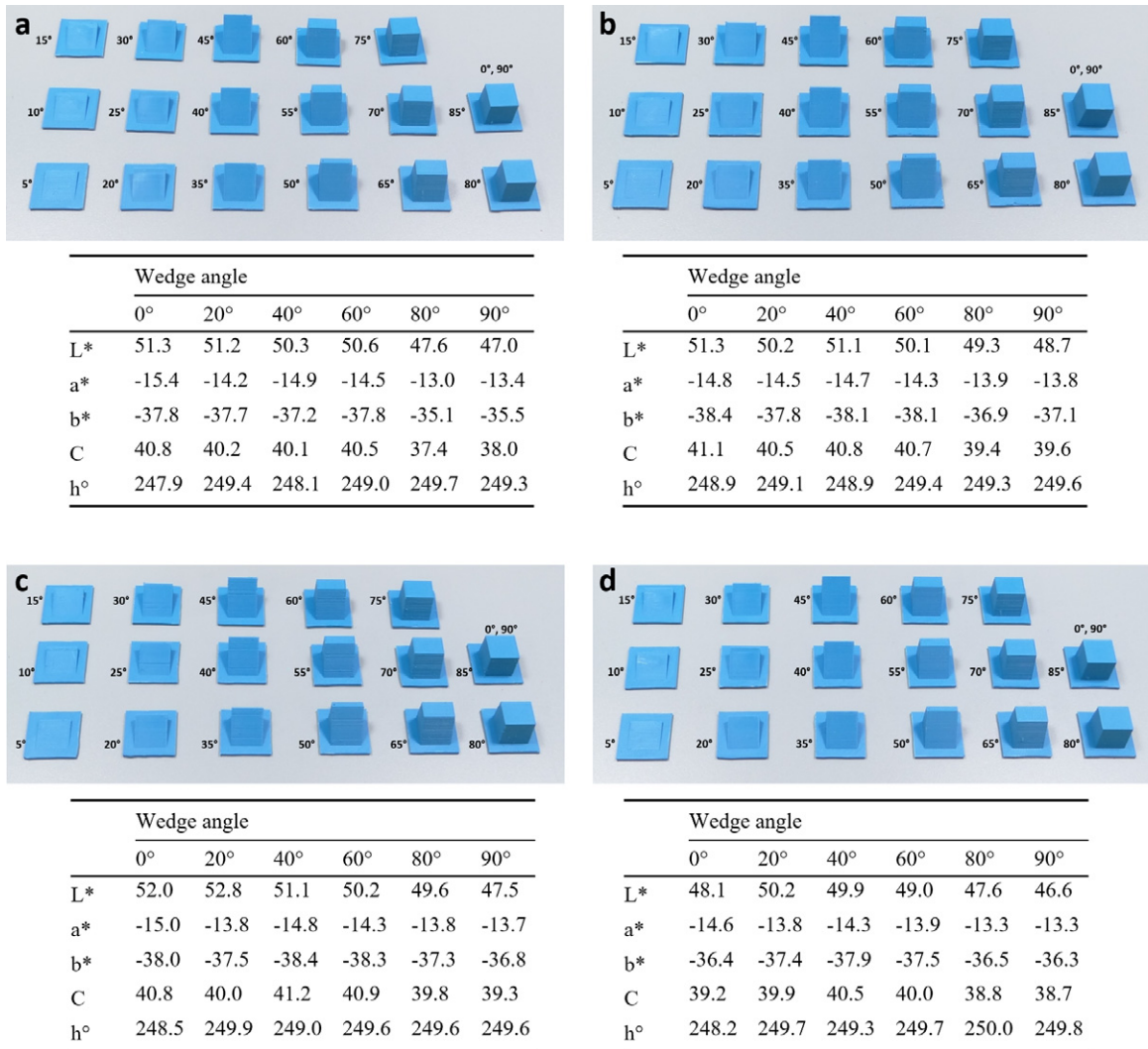|	Wedge angle					
	0°	20°	40°	60°	80°	90°
L*	48.1	50.2	49.9	49.0	47.6	46.6
a*	-14.6	-13.8	-14.3	-13.9	-13.3	-13.3
b*	-36.4	-37.4	-37.9	-37.5	-36.5	-36.3
C	39.2	39.9	40.5	40.0	38.8	38.7
h°	248.2	249.7	249.3	249.7	250.0	249.8

Figure 8. Photograph and color characteristics of cyan surfaces under a D50 illumination at different infill densities: (a) 0, (b) 30, (c) 60, and (d) 90%.
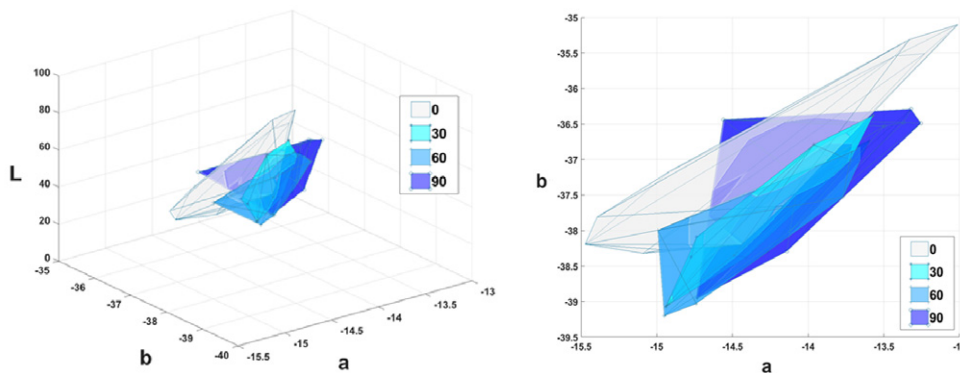

Figure 9. The color gamut of the cyan samples at different infill densities (%).

The average $L*a*b*$ values for each wedge were used to calculate the CIEDE2000 color difference to identify the color difference between each sample group. The average measured reflectance of the wedge of 0° (the flat horizontal zone) is called the reference value for each sample. According to the opponent-colors theory of color vision expressed in CIELAB, L defines lightness, and $a*$ denotes the red/green value, and $b*$ the yellow/blue value. Figure 11 shows
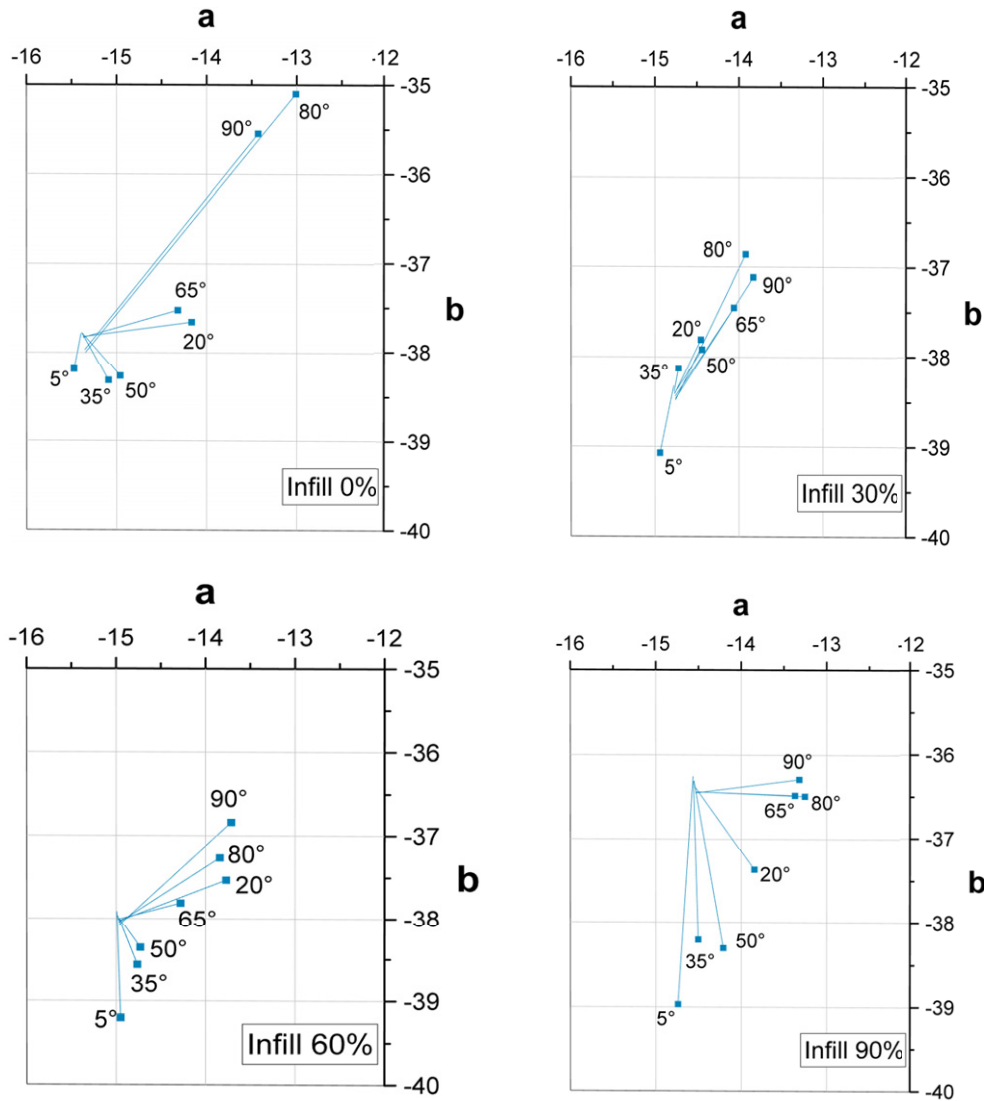
Figure 10. $L^*a^*b^*$ values of selected wedge angles of the cyan samples at different infill densities. The attached lines represent the CIEDE2000 value and direction, corresponding to the reference angle of 0°.

CIEDE2000 results from cyan samples assessed under the same appearance measurement condition. In general, the trend in CIEDE2000 values reveals that the higher infill density gives the most significant color difference at a wedge angle $< 60°$. At higher angles, however, the trend is reversed, that is, the zero-infill density displayed the highest color variation, except at 90°, where the 60% infill had a slightly higher value. In total, 30% infill appeared to represent more stable results concerning the color attribute of cyan samples, particularly at low wedge angles. Furthermore, the slope ranges from 40° to 65° meant a small threshold of color difference.

Measurements for the dull red samples resulted in a similar trend in the spectral (lightness shift in Figure 12), and the chromaticity coordinates based on the 1931 CIE (distribution of results in Figure 13). Again, the diagram shifted to the lower reflectance values for higher wedge angles at different infill levels. The range of spectral values was roughly the same between 5 and 60%.

The zero-infill samples indicated a loose convergence of the x and y results in terms of the distribution of chromaticity values (Figures 13 and 14). Similar to the cyan samples, the distribution of the $x-y$ values for sloping surfaces did not follow a certain pattern. It may suggest that although the stability of the color is noticeable on a flat FDM surface, reproducing the color is difficult for the inclined surface. It is not only because of the presence of layers and physical irregularities on the extrusion-based AM surfaces, but also it can be because of the color inconsistency in the filaments as the general feedstock for FDM printers.

Color characteristics and color gamut in Figures 15–17 indicate that the color change in the a^*b^*-plane for higher wedge angles is generally more extensive than the lower angles at different infill densities. The variation in the lightness (L^*) played the main role in the color difference on wedges for both samples.
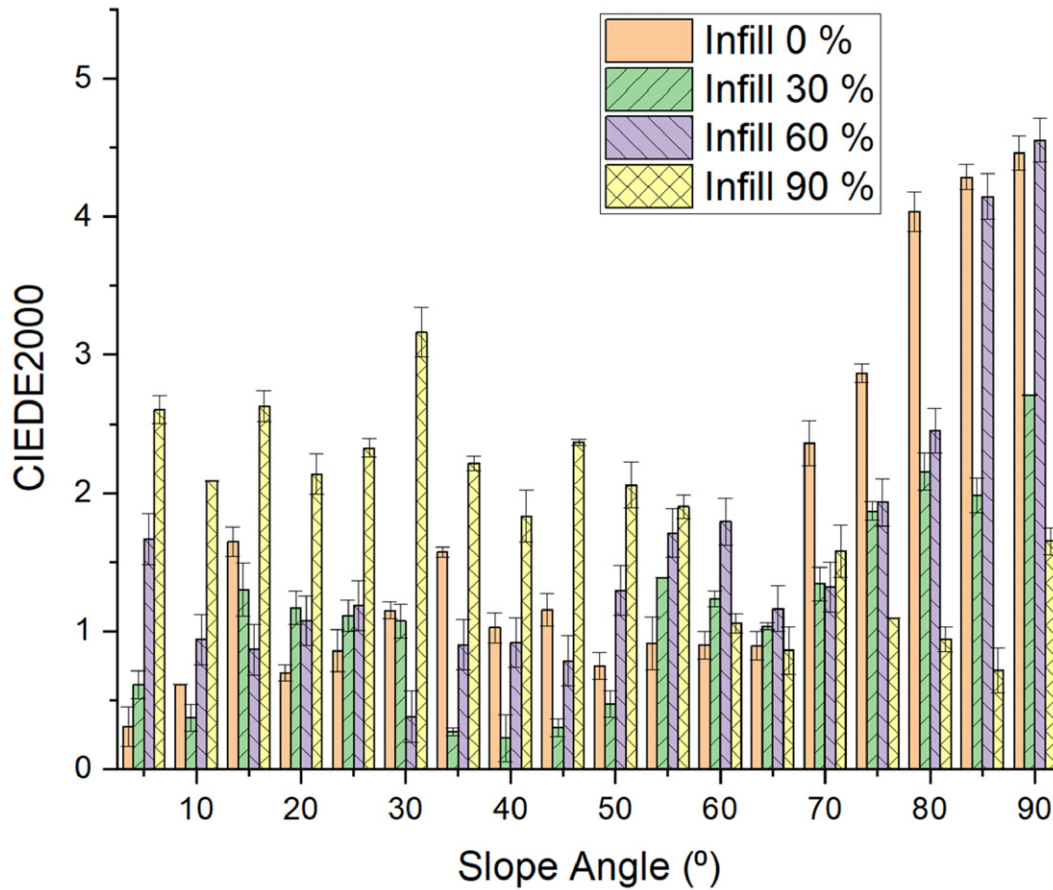
Figure 11. Average MCDM values of CIEDE2000 color difference and the corresponding RMSE for cyan samples at different infill densities.
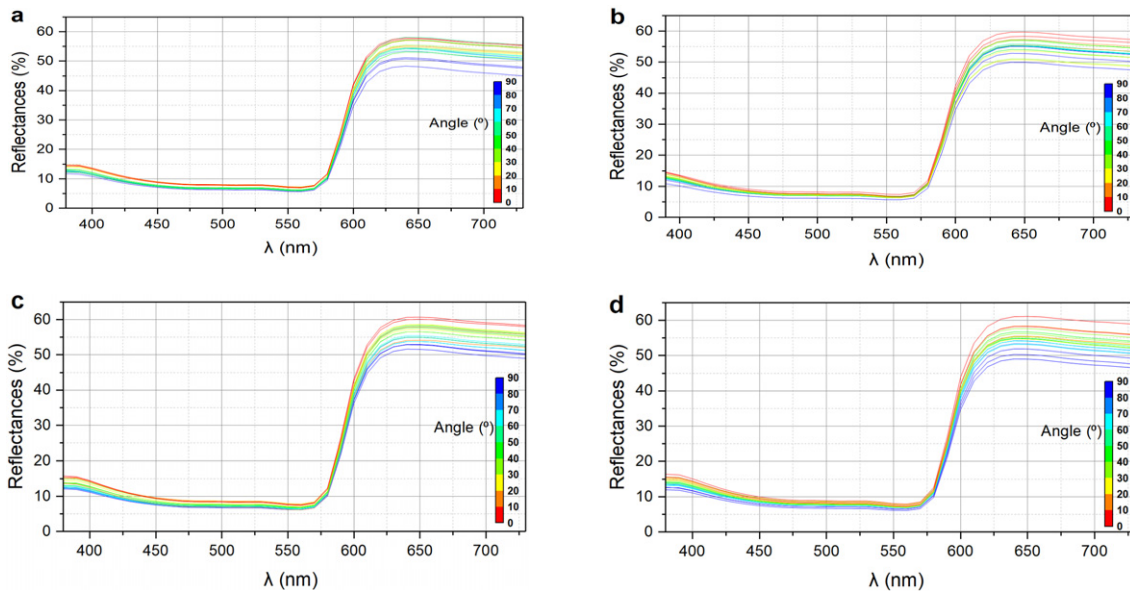

Figure 12. Reflectance spectra of dull red FDM specimens at different infill densities: (a) 0, (b) 30, (c) 60, and (d) 90%.

The CIEDE2000 results from the dull red samples in Figure 18 suggested an incremental trend in the color difference in the upper wedge angles. However, the average value of color differences indicated that the unfilled samples had more color differences (Figure 19). Generally, it can be seen from the average CIDE2000 for different infill values that the higher density inside the FDM parts is associated with higher color differences. However, the correlation
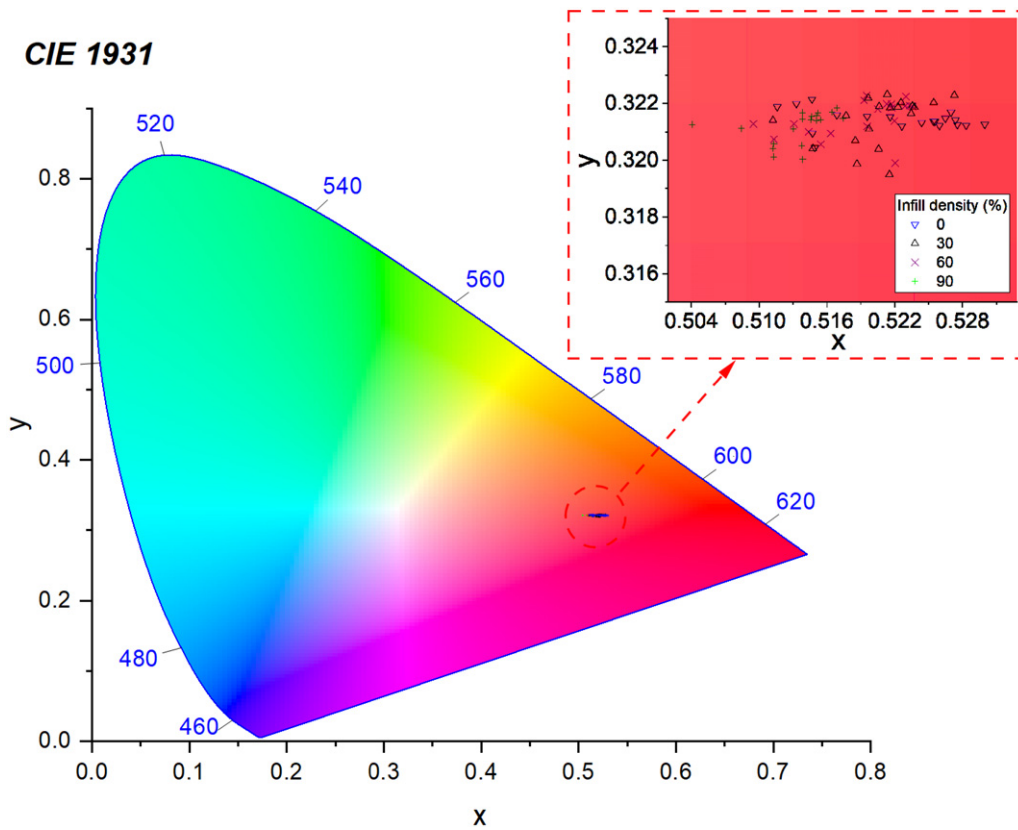
Figure 13. The enlarged and the chromaticity coordinates of the dull red samples at different wedges according to the CIE 1931 $x-y$ chromaticity diagram (D50).
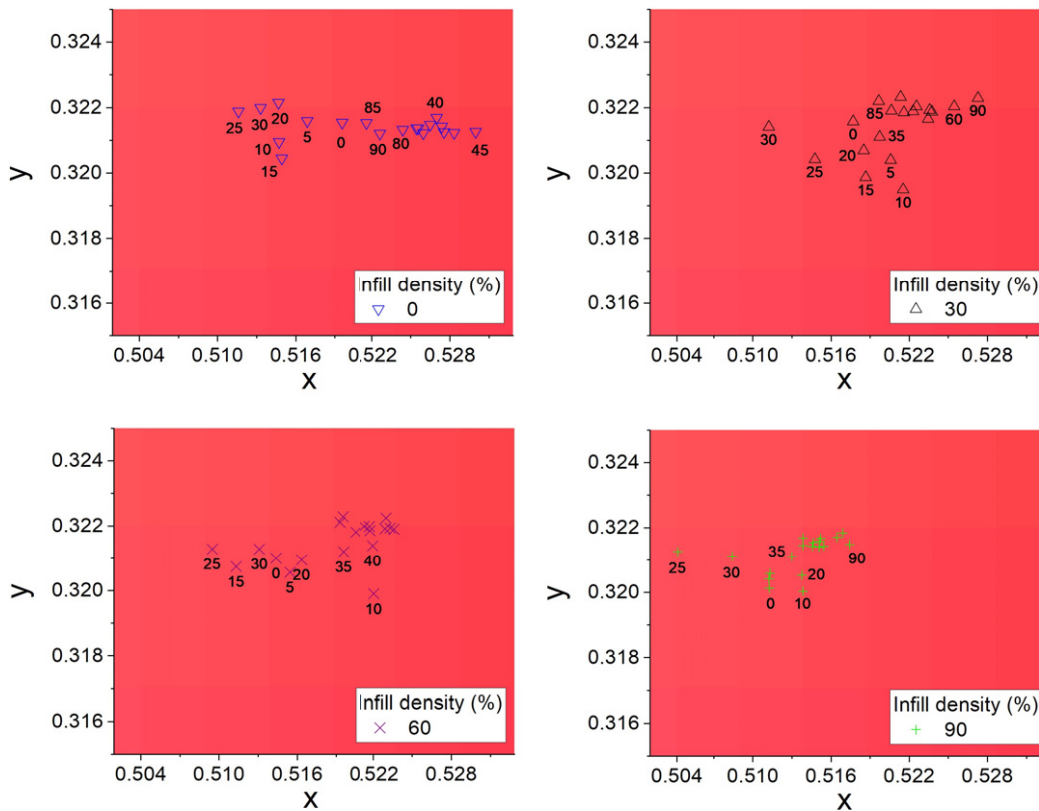

Figure 14. The chromaticity coordinates of the dull red samples at different infill densities according to the CIE 1931 $x-y$ chromaticity diagram (D50).
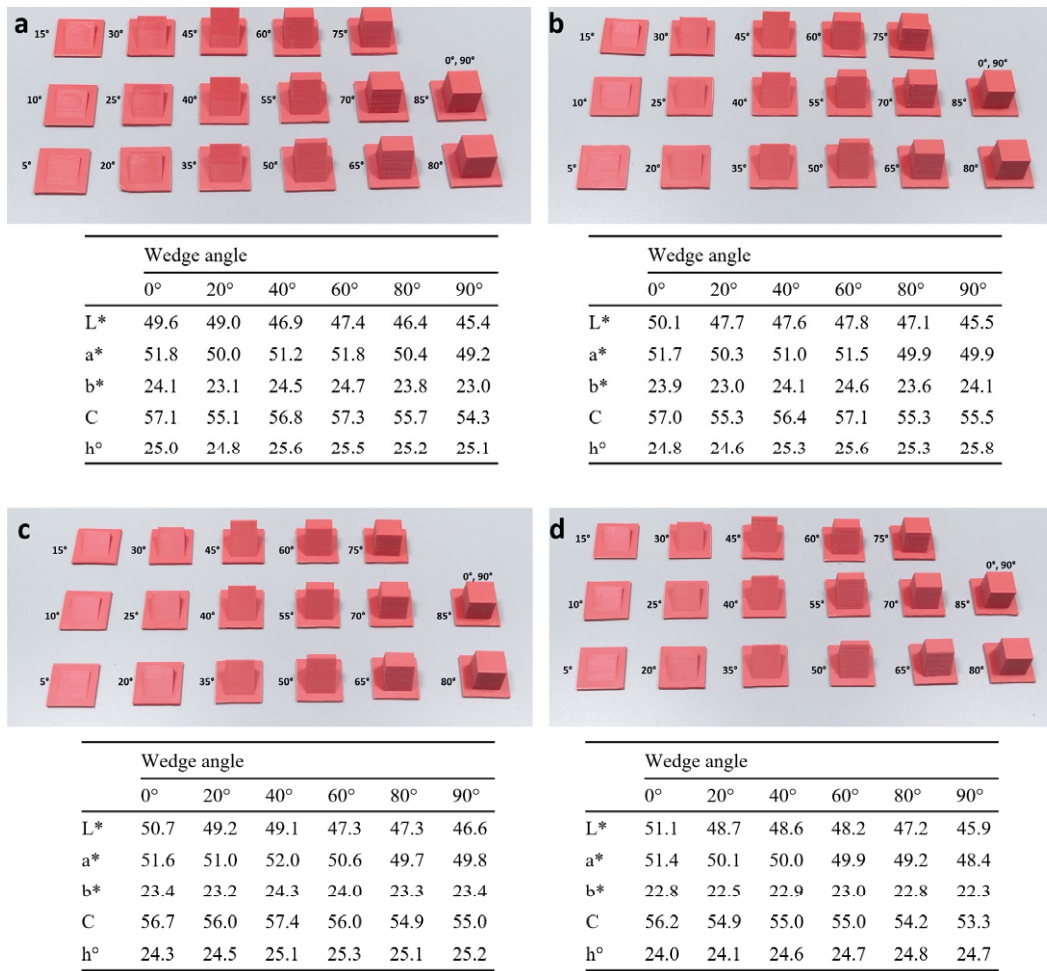
Figure 15. Photograph and color characteristics of dull red surfaces under a D50 illumination at different infill densities: (a) 0, (b) 30, (c) 60, and (d) 90%.
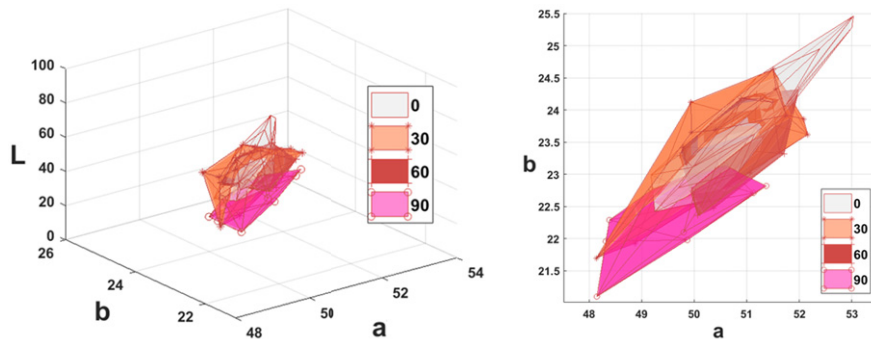
(a)

	Wedge angle					
	0°	20°	40°	60°	80°	90°
L*	49.6	49.0	46.9	47.4	46.4	45.4
a*	51.8	50.0	51.2	51.8	50.4	49.2
b*	24.1	23.1	24.5	24.7	23.8	23.0
C	57.1	55.1	56.8	57.3	55.7	54.3
h°	25.0	24.8	25.6	25.5	25.2	25.1

(b)

	Wedge angle					
	0°	20°	40°	60°	80°	90°
L*	50.1	47.7	47.6	47.8	47.1	45.5
a*	51.7	50.3	51.0	51.5	49.9	49.9
b*	23.9	23.0	24.1	24.6	23.6	24.1
C	57.0	55.3	56.4	57.1	55.3	55.5
h°	24.8	24.6	25.3	25.6	25.3	25.8

(c)

	Wedge angle					
	0°	20°	40°	60°	80°	90°
L*	50.7	49.2	49.1	47.3	47.3	46.6
a*	51.6	51.0	52.0	50.6	49.7	49.8
b*	23.4	23.2	24.3	24.0	23.3	23.4
C	56.7	56.0	57.4	56.0	54.9	55.0
h°	24.3	24.5	25.1	25.3	25.1	25.2

(d)

	Wedge angle					
	0°	20°	40°	60°	80°	90°
L*	51.1	48.7	48.6	48.2	47.2	45.9
a*	51.4	50.1	50.0	49.9	49.2	48.4
b*	22.8	22.5	22.9	23.0	22.8	22.3
C	56.2	54.9	55.0	55.0	54.2	53.3
h°	24.0	24.1	24.6	24.7	24.8	24.7

Figure 16. The color gamut of the dull red samples at different infill densities (%).

between the mean color difference and wedge angle in both cyan and dull red samples is not linear. The number of layers, the staircase effect, and the random errors due to variation in printing conditions can affect the layered microstructures significantly [42].

In particular, the formation of stairs is an inherent issue with the FDM method and affects surface quality

significantly in comparison with traditional manufacturing techniques such as injection molding [31, 42]. For instance, while there was only a base layer at the flat surface, it reached 18, 37, 57, 78, 99, 123, 150, and 179 layers for wedge angles from 5° to 40°, consecutively. Then it is limited to the maximum 214 layers for 45° to 90° samples. In this case, the horizontal width of stairs was 0.83, 0.41, 0.26, 0.19, 0.15, 0.12,
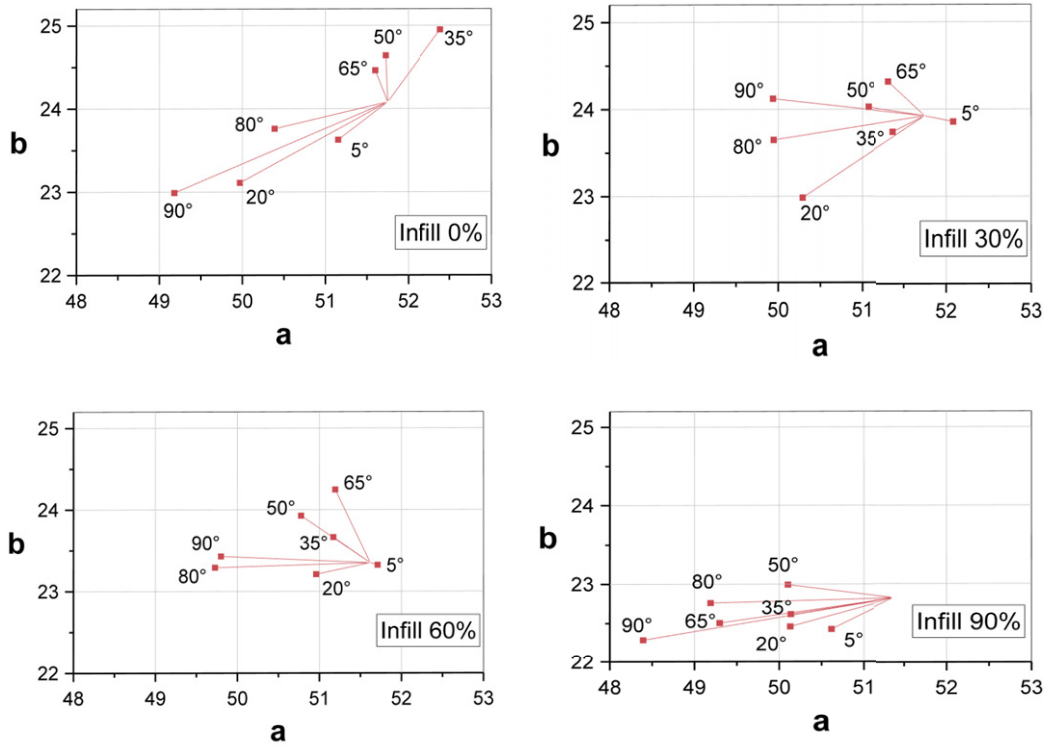
Figure 17. $L^*a^*b^*$ values of selected wedge angles of the red samples at different infill densities. The attached lines represent the CIEDE2000 value and direction, corresponding to the reference angle of 0°.
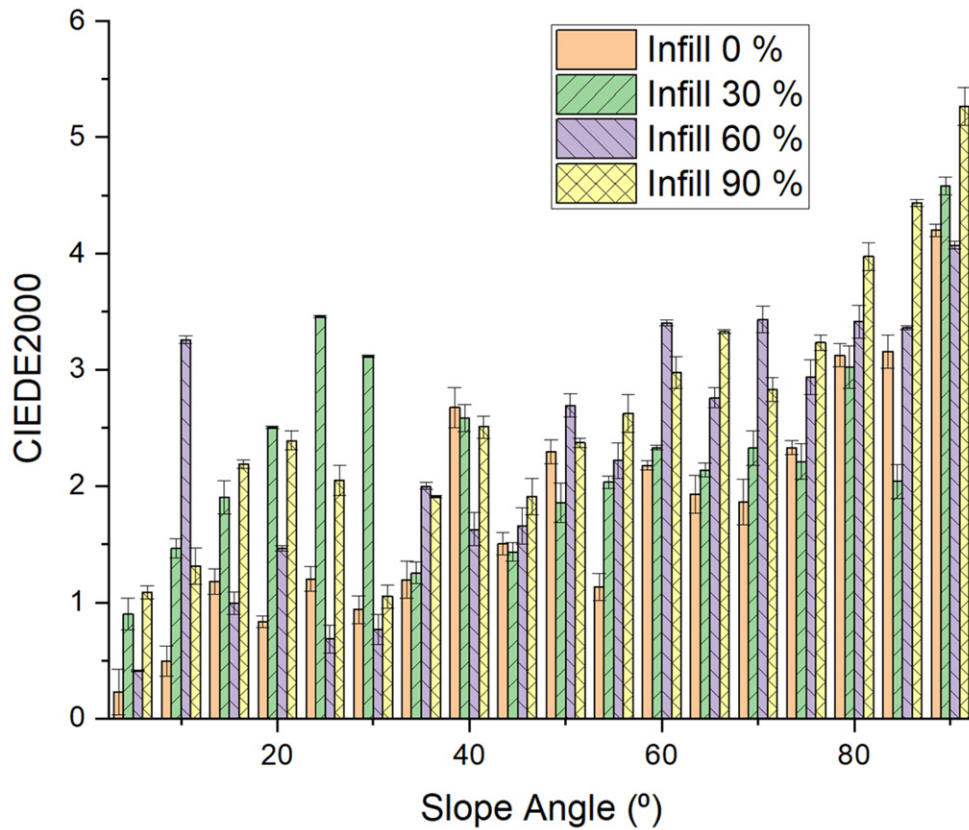

Figure 18. The MCDM value of CIEDE2000 color difference and the corresponding RMSE for dull red samples at different infill densities.
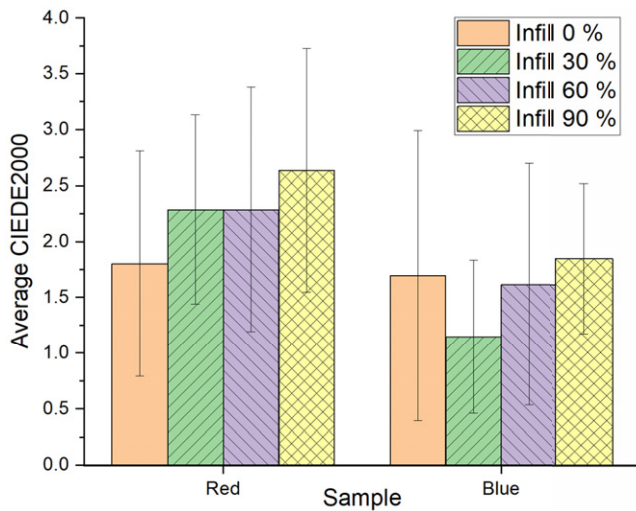
Figure 19. The MCDM CIEDE2000 color difference for each set of measurements. Each column bar represents an average value for color difference in wedge angles between 0° to 90° at intervals of 5°.

0.10, 0.08 mm for wedge angles from 5° to 45°, consecutively. It reached a value less than the layer thickness (0.07 mm) at 50°, where the horizontal width of stairs started to decrease to 0.06, 0.05, 0.04, 0.03 mm for 55° to 70°, consecutively. For the rest angles, it was less than 0.03 mm.

Although there was a meaningful association between the variations in staircase effect and the wedge angles as expected, the correlation between slope angles and color differences was non-linear due to many influential printing factors. In particular, environmental factors can impose irregularities on the surface, resulting in a rougher surface, which consequently can affect the spectral results. It includes variation in temperature, humidity, platform vibration, airflow, dust particles, etc. [25, 43].

Regarding the infill 0%, a small bump was observed at lower wedge angles in some cyan samples, resulting from incubating hot air in the surface elements during the printing process at temperature of 215°C. These bumps could affect the color difference results and explain the irregularity in the color of the unfilled samples of the cyan parts.

The notable RMSE errors in the color difference resulted from the uncertainty raised by the layer-upon-layer nature of FDM 3D printing. Considering the role of wedge angles in the design step, the polynomial fitting results with 95% confidence in Figure 20 suggest that the color difference increases exponentially at higher wedge angles. In particular, the wedge angles of 80° to 90° for the two filaments showed a significant color difference. According to the CIEDE2000 formula [11, 12], the color difference of 1 is generally considered unnoticed and barely perceptible by the average human observer. An experienced observer can only notice ΔE between 1 and 2. In the case of $2 < \Delta E_{ab}^* < 3.5$, the difference is also noticed by an inexperienced observer. The difference is noticeable in the range of 3.5 to 5, and $\Delta E_{ab}^* < 6$

is typically considered an acceptable match in commercial reproduction in printing presses. Regarding human vision, it is more sensitive to color differences if two colors actually touch each other [40, 44]. According to the calculated color difference in Fig. 20, ΔE_{ab}^* ranges were less than 5 for all samples. It means the maximum color difference is possible to be noticed by an inexperienced observer for high wedge angles. However, it is not easy to recognize the appearance difference due to the color in the case of lower wedge angles. Considering the intrinsic errors due to the measuring device in Fig. 4 (mean $\Delta E_{ab}^* = 0.16$), the error was less than the measured minimum color difference ($\Delta E_{ab}^* = 0.22$) for both samples in dull red (infill 0% and wedge angle 5°) and cyan (infill 30% and wedge angle 40°) colors. In other words, the spectrophotometer was sufficiently accurate to record the minor color differences for microtextured samples 3D-printed by the FDM method.

The above results suggest a pathway based on the studied parameters for the simulation and design of 3D-printed objects. For instance, defining boundary conditions and constraints in a 3D design for topology optimization (TO) is a potential application as a mathematical method for increasing the performance of the machine to print optimized surfaces.

4. CONCLUSIONS

This study represented an insight into the influence of additive manufacturing pre-processing steps on the color difference of structured surfaces. For this purpose, two filament spools with different colors from the same material and manufacturer were used to print samples with different wedge angles and infill densities. The increasing CIEDE2000 values at higher wedge angles and infill densities uncovered an idea to optimize the design and select the best printing process for the feature FDM printing. As indicated in this study, while the measurements of the color difference were unstable because of the layer-by-layer nature of the AM objects, it is possible to evaluate the appearance using standard spectrophotometers. The color attribute has been examined among other appearance properties, by measuring tristimulus values of a color stimulus. According to the results, the change in the lightness (L^*) played the main role in the color variation on the wedges. The variation in staircase effect corresponding to the wedge angles had a significant correlation. It was revealed that the lower reflectance at the higher wedge angle was mainly due to the smaller horizontal width of stairs. Experimental work revealed the color cyan PLA filaments can offer a more stable color during manufacturing, which means that the filament color can affect the appearance of the same feedstock material. However, the dominant factor for the color difference was the layers formation and the staircase effect. Overall, the discussed results are instrumental in altering the color appearance of printed parts deliberately by means of controlling the generation of surface texture in the pre-processing stage in the case of PLA filaments. It suggests a possibility to generate micro-textures at lower
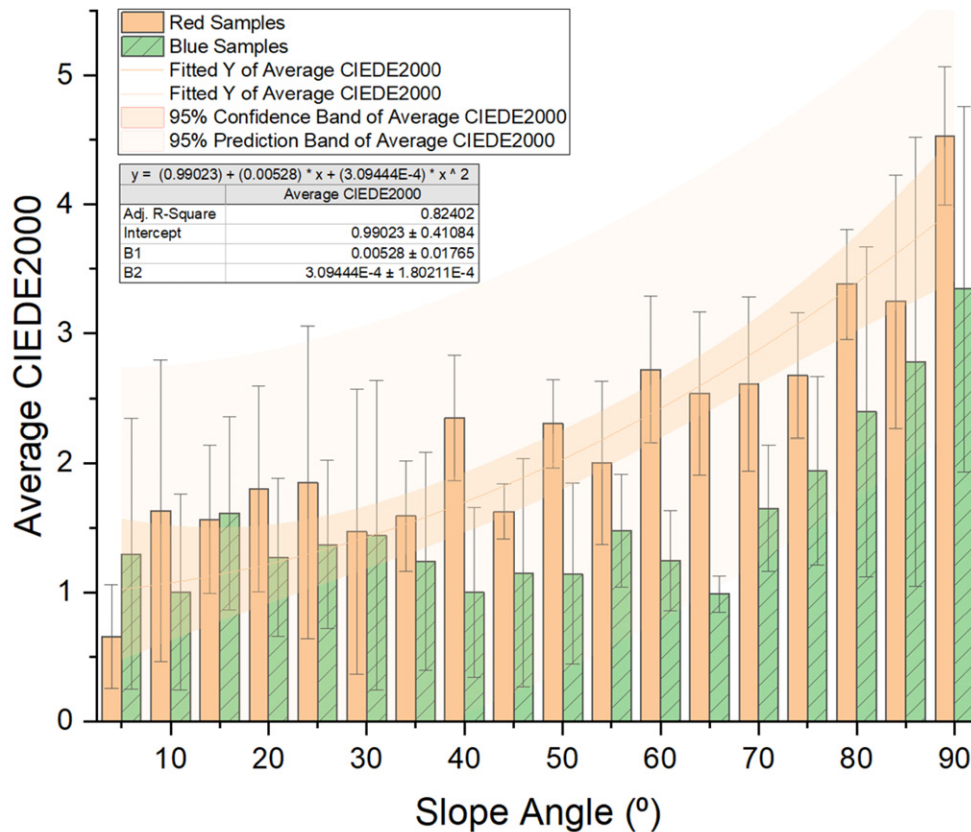
Figure 20. 95th percentile polynomial fitting results for cyan and dull red PLA samples at different wedge angles.

wedge angles and fewer infill densities for PLA filaments through topological optimization and generative designs.

REFERENCES
[1] J. Yuan, M. Zhu, B. Xu, and G. Chen, "Review on processes and color quality evaluation of color 3D printing," Rapid Prototyping J. **24**, 409–415 (2018).
[2] K. Xiao, A. Sohiab, P. Sun, J. M. Yates, C. Li, and S. Wuerger, "A colour image reproduction framework for 3D colour printing," Proc. SPIE **10153**, 1015318 (2016).
[3] S. R. Mogali, W. Y. Yeong, H. K. J. Tan, G. J. S. Tan, P. H. Abrahams, N. Zary, N. Low-Beer, and M. A. Ferenczi, "Evaluation by medical students of the educational value of multi-material and multi-colored three-dimensional printed models of the upper limb for anatomical education," Anat. Sci. Educ. **11**, 54–64 (2018).
[4] M. Inoue, T. Freel, A. V. Avermaete, and W. M. Leevy, "Color enhancement strategies for 3D Printing of X-ray computed tomography bone data for advanced anatomy teaching models," Appl. Sci. **10**, 1571 (2020).
[5] L. Ding, W. Lu, J. Zhang, C. Yang, and G. Wu, "Preparation and performance evaluation of duotone 3D-printed polyetheretherketone as oral prosthetic materials: A proof-of-concept study," Polymers **13**, 1949 (2021).
[6] J. Weiler and S. Kuznetsov, "Crafting colorful objects: A DIY method for adding surface detail to 3D prints," Proc. Conf. on Human Factors in Computing Systems (ACM, New York, NY, 2017), pp. 2217–2223.
[7] J. Yuan, J. Tian, C. Chen, and G. Chen, "Experimental investigation of color reproduction quality of color 3D printing based on colored layer features," Molecules **25**, 2909 (2020).
[8] G. Chen, X. Wang, H. Chen, and C. Chen, "Realization of rapid large-size 3D printing based on full-color powder-based 3DP technique," Molecules **25**, 2037 (2020).
[9] X. Wang, G. Chen, J. Yuan, and L. Cai, "Research on cutting-bonding process of powder based 3D printing model," Lecture Notes in Electrical Engineering (Springer, Berlin, Heidelberg, 2019), pp. 495–500.
[10] J. Tian, J. Yuan, H. Li, D. Yao, and G. Chen, "Advanced surface color quality assessment in paper-based full-color 3D printing," Materials **14**, 1–13 (2021).
[11] X. Yan, J. Yuan, and G. Chen, "Applications analysis of paper-based color 3D printing in the map industry," Lecture Notes in Electrical Engineering (Springer, Berlin, Heidelberg, 2018), pp. 377–383.
[12] M. Cui, X. Li, G. Wu, and Q. Cao, "Measurement and evaluation of the surface color of 3D paper product," Lecture Notes in Electrical Engineering (Springer, Berlin, Heidelberg, 2019), pp. 108–113.
[13] J. Yuan, J. Tian, D. Yao, and G. Chen, "Color assessment of paper-based color 3D prints using layer-specific color 3D test charts," Lecture Notes in Electrical Engineering (Springer, Berlin, Heidelberg, 2021), pp. 123–131.
[14] J. Yuan, L. Cai, X. Wang, and G. Chen, "Visualization of biomedical products based on paper-based color 3D printing," Proc. IS&T Printing for Fabrication 2019 (IS&T, Springfield, VA, 2019), pp. 128–131.

15 D. Buchbinder, H. Schleifenbaum, S. Heidrich, W. Meiners, and J. Bültmann, "High power selective laser melting (HP SLM) of aluminum parts," Phys. Procedia **12**, 271–278 (2011).

16 J. Gu, B. Liu, H. Yang, and X. Li, "A fast and CMP-free TSV process based on wafer-level liquid-metal injection for MEMS packaging," *2016 IEEE 29th Int'l. Conf. on Micro Electro Mechanical Systems (MEMS)* (IEEE, Piscataway, NJ, 2016), pp. 569–572.

17 H. M. Wang, G. X. Chen, and W. B. Zhang, "3D printing of topographic map based on UV ink-jet printer," *Applied Mechanics and Materials* (Trans Tech Publ, Baech, Switzerland, 2014), Vol. 469, pp. 309–312.

18 J. Yang, L. W. Wu, and J. Liu, "Rapid prototyping and fabrication method for 3-D food objects," US Patent 6,280,785 (2001).

19 K. Xiao, F. Zardawi, R. van Noort, and J. M. Yates, "Color reproduction for advanced manufacture of soft tissue prostheses," J. Dent. **41**, e15–e23 (2013).

20 A. Sohaib, K. Amano, K. D. Xiao, J. M. Yates, C. Whitford, and S. Wuerger, "Colour quality of facial prostheses in additive manufacturing," Int. J. Adv. Manuf. Technol. **96**, 881–894 (2018).

21 P. L. Sun and Y. P. Sie, "Color uniformity improvement for an inkjet color 3D printing system," *IS&T Electronic Imaging: Color Imaging XXI: Displaying, Processing, Hardcopy, and Applications* (IS&T, Springfiled, VA, 2016), pp. COLOR-342.1–COLOR-342.6.

22 C. Li, L. Zheng, and Y. Xiao, "Study on the influencing factors of color reproduction in color 3D printing," *Lecture Notes in Electrical Engineering* (Springer, Berlin, Heidelberg, 2020), pp. 156–163.

23 K. Xiao, F. Zardawi, R. V. Noort, and J. M. Yates, "Developing a 3D colour image reproduction system for additive manufacturing of facial prostheses," Int. J. Adv. Manuf. Technol. **70**, 2043–2049 (2014).

24 H. Li, T. Wang, J. Sun, and Z. Yu, "The effect of process parameters in fused deposition modelling on bonding degree and mechanical properties," Rapid Prototyping J. **24**, 80–92 (2018).

25 S. Vyavahare, S. Teraiya, D. Panghal, and S. Kumar, "Fused deposition modelling: a review," Rapid Prototyping J. **26**, 176–201 (2020).

26 E. H. Baran and H. Y. Erbil, "Surface modification of 3D printed PLA objects by fused deposition modeling: a review," Colloid Interfac. **3**, 25 (2019).

27 A. Yahamed, P. Ikonomov, P. D. Fleming, A. Pekarovicova, P. Gustafson, A. Q. Alden, and S. Alrafeek, "Mechanical properties of 3D printed polymers," J. Print Media Technol. Res. **5**, 273–289 (2016).

28 A. Yahamed, P. Ikonomov, P. D. Fleming, A. Pekarovicova, and P. Gustafson, Designed structures for bone replacement, "Designed structures for bone replacement," J. Print Media Technol. Res. **5**, 291–307 (2016).

29 A. Yahamed, M. Joyce, P. D. Fleming, A. Pekarovicova, and P. Ikonomov, "Polymers for 3D printed structures, precision, topography and roughness," Int. J. Multidisciplinary Res. Studies **1**, 43–59 (2018).

30 D. J. Roach, C. Roberts, J. Wong, X. Kuang, J. Kovitz, Q. Zhang, T. G. Spence, and H. J. Qi, "Surface modification of fused filament fabrication (FFF) 3D printed substrates by inkjet printing polyimide for printed electronics," Addit. Manuf. **36**, 101544 (2020).

31 M. Taufik and P. K. Jain, "Part surface quality improvement studies in fused deposition modelling process: a review," Aust. J. Mech. Eng. **13**, 1–25 (2020).

32 A. K. Sood, R. Ohdar, and S. S. Mahapatra, "Improving dimensional accuracy of fused deposition modelling processed part using grey Taguchi method," Mater. Des. **30**, 4243–4252 (2009).

33 S. Masood, W. Rattanawong, and P. Iovenitti, "A generic algorithm for a best part orientation system for complex parts in rapid prototyping," J. Mater. Process. Technol. **139**, 110–116 (2003).

34 Y.-S. Liao and Y.-Y. Chiu, "A new slicing procedure for rapid prototyping systems," Int. J. Adv. Manuf. Technol. **18**, 579–585 (2001).

35 M. Livesu, S. Ellero, J. Martínez, S. Lefebvre, and M. Attene, "From 3D models to 3D prints: an overview of the processing pipeline," *Comput. Graph. Forum* (Wiley Online Library, Hoboken, NJ, 2017), pp. 537–564.

36 B. N. Turner and S. A. Gold, "A review of melt extrusion additive manufacturing processes: II. Materials, dimensional accuracy, and surface roughness," Rapid Prototyping J. **21**, 250–261 (2015).

37 M. Dattner and D. Bohn, "European energy efficiency improvement by means of visualisation and benchmarking tailored to the print and media industry," International Circular of Graphic Education and Research **3**, 42–54 (2010).

38 M. R. Luo, G. Cui, and B. Rigg, "The development of the CIE 2000 colour-difference formula: CIEDE2000, Color Research & Application: Endorsed by Inter-Society Color Council, The Colour Group (Great Britain), Canadian Society for Color, Color Science Association of Japan, Dutch Society for the Study of Color, The Swedish Colour Centre Foundation, Colour Society of Australia," Centre Français de la Couleur **26**, 340–350 (2001).

39 G. A. Klein and T. Meyrath, *Industrial Color Physics* (Springer, Berlin, Heidelberg, 2010).

40 W. Mokrzycki and M. Tatol, "Colour difference ΔE – A survey," Machine Graphics and Vision **20**, 383–411 (2011).

41 P. Green, *A Colour Engineering Toolbox* (John Wiley & Sons, Hoboken, NJ, 2003).

42 A. D. Valino, J. R. C. Dizon, A. H. Espera Jr., Q. Chen, J. Messman, and R. C. Advincula, "Advances in 3D printing of thermoplastic polymer composites and nanocomposites," Prog. Polym. Sci. **98**, 101162 (2019).

43 S. D. Nath and S. Nilufar, "An overview of additive manufacturing of polymers and associated composites," Polymers **12**, 2719 (2020).

44 J. Schanda, *Colorimetry: Understanding the CIE System* (John Wiley & Sons, Hoboken, NJ, 2007).